



Degree Project in Technology

First cycle, 15 credits

# Numerical Solutions and Parameter Sensitivity of the Lorenz System

VILMER STRÖM

EIRA LARSSON

# **Abstract**

In chaos theory there are many different problems still unsolved. One of which is the optimization of infinite time average functionals on manifolds. To try one of the different tools to solve this problem we want to find stable manifolds in chaotic dynamical systems. In this thesis we find different manifolds for the Lorenz system when using a time dependent  $\mu$  parameter and perform a sensitivity analysis on some of them. The existence of these manifolds are motivated numerically with the help of the shadowing lemma and extensive comparison of different numerical solvers.

# **Keywords**

Lorenz system, Dynamic Bifurcation, Periodic Parameter Perturbation, Chaos, Runge-Kutta, Shadowing Lemma.

## **Acknowledgements**

We express our gratitude to our supervisor, Pritpal Matharu, for identifying an engaging topic for our Bachelor Thesis and for providing invaluable guidance throughout our journey. Furthermore, we would like to acknowledge the significant contribution of OpenAI's chat GPT, which greatly aided us in improving a substantial portion of the text.

## **Authors**

Vilmer Ström <[vilmers@kth.se](mailto:vilmers@kth.se)> and Eira Larsson <[eiral@kth.se](mailto:eiral@kth.se)>  
Numerical Analysis  
KTH Royal Institute of Technology

## **Place for Project**

Stockholm, Sweden

## **Examiner**

Sara Zahedi  
Numerical Analysis  
KTH Royal Institute of Technology

## **Supervisor**

Pritpal Matharu  
Numerical Analysis  
KTH Royal Institute of Technology

# Contents

<b>1</b>	<b>Introduction</b>	<b>1</b>
<b>2</b>	<b>The Lorenz System</b>	<b>3</b>
<b>3</b>	<b>Shadowing Lemma</b>	<b>4</b>
<b>4</b>	<b>Numerical Solvers</b>	<b>5</b>
4.1	Euler Forward . . . . .	5
4.2	Runge-Kutta Method of order four (RK4) . . . . .	5
4.3	Multi-step differential transformation method . . . . .	6
4.4	Rodas5 and RadauIIA5 . . . . .	6
<b>5</b>	<b>Numerical Methods</b>	<b>7</b>
5.1	Numerical Solvers . . . . .	7
5.2	Comparison of Numerical solvers . . . . .	7
5.3	Time dependent $\mu$ . . . . .	11
5.4	Perturbations and stability of manifolds . . . . .	11
<b>6</b>	<b>Results</b>	<b>13</b>
6.1	Parameter selection . . . . .	13
6.2	Comparison Numerical Solvers . . . . .	14
6.3	Finding manifolds and perturbing them . . . . .	17
6.4	Sensitivity analysis of manifolds . . . . .	20
<b>7</b>	<b>Discussion</b>	<b>22</b>
7.1	Comparison Numerical Solvers . . . . .	22
7.2	Finding manifolds and perturbing them . . . . .	24
7.3	Sensitivity analysis of manifolds . . . . .	24
<b>8</b>	<b>Future Work</b>	<b>25</b>
<b>References</b>		<b>26</b>

# 1 Introduction

Dynamical systems are models designed to describe how different state variables evolve over time and how they affect the system as a whole. They are used in various fields including, but not limited to: classical mechanics, chemical kinetics, population biology, and many more [11].

In 1963, mathematician and meteorologist Edward Lorenz, with the help of computer scientist Ellen Fetter, developed a simplified model of atmospheric convection rolls [4]. This model, known as the Lorenz system, consists of three ordinary differential equations,

$$\begin{cases} \frac{dx}{dt} = \theta(y(t) - x(t)), \\ \frac{dy}{dt} = x(t)(\mu - z(t)) - y(t), \\ \frac{dz}{dt} = x(t)y(t) - \beta z(t). \end{cases} \quad (1)$$

Where we define  $\vec{u}(t)$  as  $\vec{u}(t) := [x(t), y(t), z(t)]$  on the closed time interval  $t \in [0, T]$ . The Lorenz system is deterministic and *chaotic* over a wide range of parameter values. A chaotic system is very sensitive to the initial conditions, making long-term predictions impossible. However, Lorenz was able to observe a kind of structure to the chaos, as the solutions settle onto a parameter-dependent set in space, called an attractor [4, 11].

Since Lorenz's work, extensive research has been done on the Lorenz system and many similar chaotic systems. Many articles have been written about the Lorenz system in particular, some of which are focusing on finding patterns in the chaos, to determine what predictability there exists, and others on trying to control it.

An interesting optimization problem that this project serves as a foundation for is the minimization of a cost functional,  $\mathcal{J}(\phi(s))$ , defined as the limit of the integral of a function  $\mathcal{J}(\vec{u}(t), \phi(s))$  over time. Where  $\phi(s)$  is an infinite-dimensional parameter, belonging to the set  $\mathcal{X}$ . Specifically, the problem aims to minimize  $\mathcal{J}(\phi)$  subject to the constraint  $C(\vec{u}(\phi), \phi) = 0$ , where the constraint is defined by the manifold  $\mathcal{M} = \{\phi \in \mathcal{X} : C(\vec{u}(\phi), \phi) = 0\}$  [5].

In this project we will find different manifolds and investigate their stability. These manifolds could later be used for testing optimization schemes on problems like the one

described above.

## 2 The Lorenz System

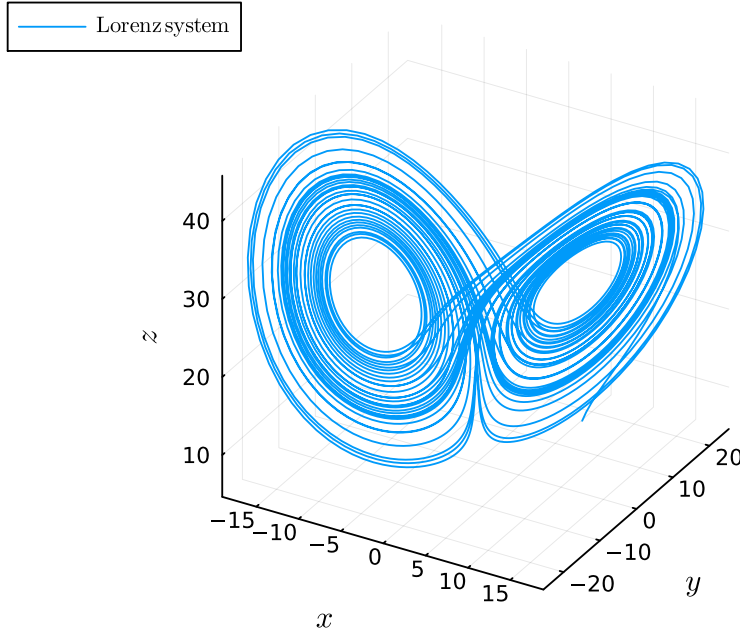


Figure 2.1: An image of the strange attractor when  $\theta = 10$ ,  $\beta = 8/3$  and  $\mu = 28$ .

The Lorenz system is a dynamical system on the form  $\frac{d\vec{u}}{dt} = \vec{f}(\vec{u})$  in  $\mathbb{R}^3$ . Here,  $\vec{u}$  represents the position in the phase space, and  $\frac{d\vec{u}}{dt}$  represents its velocity, collectively referred to as the *phase* [4, 9]. When starting from a given point  $\vec{u}$ , the system follows a trajectory in the phase space denoted by  $\vec{u}(t)$ . The Lorenz system is a system of ordinary differential equations as described in eq. (1).

In the system system  $\theta$ ,  $\mu$  and  $\beta$  are parameters.  $\theta$  is called a Prandtl number and  $\mu$  is called a Rayleigh number [11]. As we can observe the system has two quadratic terms  $xz$  and  $xy$  making it nonlinear. The Lorenz system is also symmetric in the sense that if  $(x(t), y(t), z(t))$  is a solution, so is  $(-x(t), -y(t), z(t))$ . The dynamics of the system are dependent on the choice of parameters, in particular the choice of the Prandl number  $\mu$ . The Prandl number affects many aspects of the system but in this report we will focus on how it affects the *fixed points*. A *fixed point*  $u^*$  is a point in space such that  $\vec{f}(u^*) = 0$ , meaning the trajectory will stay at  $u^*$  as  $t \rightarrow \infty$  [11]. For  $\mu > 1$  the system has three *fixed points*.  $(0, 0, 0)$  as well as the two fixed points  $x = y = \pm\sqrt{\beta(\mu - 1)}$ ,  $z = \mu - 1$ . For  $\mu < 1$  the origin is *globally stable* meaning that every trajectory in phase space approaches the origin as  $t \rightarrow \infty$ . When  $\mu > \frac{\theta(\theta+\beta+3)}{\theta-\beta-1}$  the system is *chaotic* and has a *strange attractor* as depicted in fig. 2.1. When the Lorenz system is chaotic numerical estimations tend to

diverge quickly from the true solution [11]. An *attractor* A is defined as follows:

1. If  $\vec{u}(0) \in A$  then  $\vec{u}(t) \in A$  for all  $t \in [0, \infty)$ .
2. There exists an open set  $U$  such that  $A \subset U$  and if  $\vec{u}(0) \in U$  then  $\min_{\vec{a} \in A} \|\vec{u}(t) - \vec{a}\| \rightarrow 0$  as  $t \rightarrow \infty$ .
3. There is no  $S \subset A$  such that  $S$  satisfies conditions 1 and 2.

If the attractor has a fractal structure it's called *strange*.

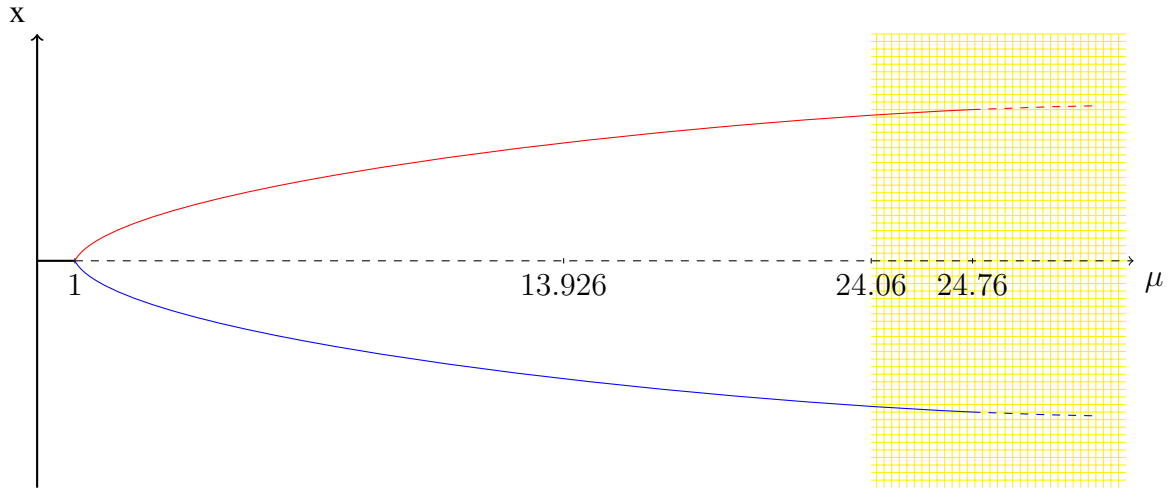


Figure 2.2: A bifurcation diagram based on the parameter value  $\mu$ . When  $\mu$  is less than 1, the origin is globally stable. In the range  $1 < \mu < 24.06$ , there exist two fixed point attractors. As  $\mu$  exceeds 13.926, the trajectories can exhibit chaotic behavior before eventually settling into one of the fixed points. For  $\mu$  greater than 24.06, a chaotic attractor emerges, resulting in three distinct attractors. However, when  $\mu$  surpasses 24.76, the fixed points cease to be attractors, and only the chaotic attractor remains [1].

### 3 Shadowing Lemma

When the Lorenz system is in a chaotic state, numerical solutions exhibit exponential divergence from the true solution. However, thanks to a lemma called the Shadowing Lemma, we know that there exists an alternative trajectory, originating from a different starting point, that closely follows the numerical trajectory. Therefore, although the numerical solution may not precisely replicate the actual trajectory, it still provides valuable insights into the behavior of the system [5, 7, 10]. Numerical solutions are useful since they can show properties of a chaotic system such as attractors. A formal definition of the Shadowing Lemma can be found in [7].

## 4 Numerical Solvers

Due to the difficulty in analytically solving systems like the Lorenz system this thesis will heavily depend on numerical approximations and numerical analysis. Part of it will therefore be to evaluate different numerical solvers through their respective approximations of the system.

Given a solution  $\vec{u}(t) : [0, T] \rightarrow \mathbb{R}^d$  to a system of ordinary differential equations  $\frac{d\vec{u}(t)}{dt} = f(\vec{u}(t), t)$ , a discretization  $\vec{u}_i = \vec{u}(t_i)$  can be introduced for a given set of  $t_i$ 's  $S = \{t_i = i \Delta t \mid i = 0, 1, \dots, N\}$ , where  $\Delta t = \frac{T}{N}$ . In this thesis we will denote a numerical approximation of the trajectory by some solver at  $t_i$  as  $\tilde{u}_i \approx \vec{u}_i$ . The collection of  $\tilde{u}_i$ 's for all  $i = 0, 1, \dots, N$  for a given approximation will be denoted as  $\tilde{u}$ .

We will discuss five different numerical solvers in this thesis: Euler Forward (EF), Runge-Kutta 4 (RK4), multi-step differential transformation method (MsDTM), Rodas5 (Ro5), and RadauIIA5 (Ra5). Rodas5 and RadauIIA5 are included in the Julia package DifferentialEquations.jl and they were chosen since they are higher tolerance stiff ODE solvers. The explicit methods Euler Forward, Runge-Kutta 4 and MsDTM were chosen because of ease of implementation even though implicit methods would be more appropriate for a chaotic system [2].

### 4.1 Euler Forward

Explicit solver of order 1. The scheme is

$$\tilde{u}_{i+1} = \tilde{u}_i + \Delta t f(\tilde{u}_i, t_i),$$

for  $i = 0, 1, \dots, N - 1$  given that  $\tilde{u}_0 = \vec{u}_0$ .

### 4.2 Runge-Kutta Method of order four (RK4)

The Runge-Kutta Methods are a family of ODE solvers where the Euler Forward method is included. The Runge-Kutta method of order four is the four step method described

below,

$$\begin{aligned}
k_1^i &= f(t_i, \tilde{u}_i), \\
k_2^i &= f\left(t_i + \frac{\Delta t}{2}, \tilde{u}_i + \frac{\Delta t}{2} k_1^i\right), \\
k_3^i &= f\left(t_i + \frac{\Delta t}{2}, \tilde{u}_i + \frac{\Delta t}{2} k_2^i\right), \\
k_4^i &= f\left(t_i + \Delta t, \tilde{u}_i + \Delta t k_3^i\right), \\
\tilde{u}_{i+1} &= \tilde{u}_i + \frac{\Delta t}{6}(k_1^i + 2k_2^i + 2k_3^i + k_4^i),
\end{aligned}$$

for  $i = 0, 1 \dots N - 1$ , given that  $\tilde{u}_0 = \vec{u}_0$ . The Runge-Kutta method of order four has been very popular due to its simplicity, ease of implementation, and the requirement of only a single initial condition. The order four in RK4 means that the global error decreases by a factor four for each halving of the step size [8].

### 4.3 Multi-step differential transformation method

Method using differential transformation technique. Scheme is

$$\tilde{u}_{i+1} = \tilde{u}_i + \sum_{k=0}^{K-1} \frac{1}{k!} \frac{d^k f}{dt^k}(\tilde{u}_i, t_i) \Delta t^{k+1}, \quad i = 0, \dots, N - 1$$

for  $i = 0, 1, \dots, N - 1$  and some choice of  $K$  given that  $\tilde{u}_0 = \vec{u}_0$ . The choice of  $K$  depends on what order is desired.

### 4.4 Rodas5 and RadauIIA5

Rodas5 is a 5th order, A-stable Rosenbrock method built into Julia's package DifferentialEquations.jl. RadauIIA5 is an A-B-L stable, 5th order Runge-Kutta method that is built into Julia's package DifferentialEquations.jl [2]. More about A-B-L stability can be found in the appendix.

## 5 Numerical Methods

### 5.1 Numerical Solvers

We implement Euler-Forward, RK4 and MsDTM but use already implemented versions of Rodas5 and RadauIIA5 from the Julia package DifferentialEquations.jl.

#### 5.1.1 Implementation of MsDTM

The transformations that are used for the Lorenz system are shown in table 5.1.

Original function	Transformation
$f(t) = u(t) \pm v(t)$	$F(k) = U(k) \pm V(k)$
$f(t) = \alpha u(t)$	$F(k) = \alpha U(k)$
$f(t) = u(t)v(t)$	$F(k) = \sum_{m=0}^k U(m)V(k-m)$

Table 5.1: Differential transformations where  $U(k) = \frac{1}{k!} \frac{d^k u}{dt^k}$  [6]

For the Lorenz system the differential transformation is

$$\begin{cases} X(k+1) = \frac{1}{k+1} [\theta Y(k) - \theta X(k)], \\ Y(k+1) = \frac{1}{k+1} \left[ \mu X(k) - \sum_{m=0}^k X(m)Z(k-m) - Y(k) \right], \\ Z(k+1) = \frac{1}{k+1} \left[ \sum_{m=0}^k X(m)Y(k-m) - \beta Z(k) \right]. \end{cases}$$

Using this transformation and notation, numerical solutions created by MsDTM will then be on the form

$$\tilde{u}_i(t) = \begin{bmatrix} \sum_{k=0}^K X_i(k)\Delta t^k \\ \sum_{k=0}^K Y_i(k)\Delta t^k \\ \sum_{k=0}^K Z_i(k)\Delta t^k \end{bmatrix}.$$

### 5.2 Comparison of Numerical solvers

To select the numerical solver for the latter parts of the project, a comparison of the solvers was conducted using four different approaches. In order to simplify the comparison, the adaptive element of the solvers from the Julia package DifferentialEquations.jl was disabled. The four comparison methods employed were:

1. Deviation from fixed points: In this preliminary comparison, the solvers were evaluated to assess their ability to remain at a fixed point. Starting from a given fixed point, the solvers were tested to determine if they could maintain their position within the fixed point over time.
2. Convergence for global stability: For a parameter set where the Lorenz system exhibits a globally stable origin, the solvers' tendency to converge to the origin was compared.
3. Energy function analysis: Changes in a defined energy function over time were examined for different parameter sets. By observing the solvers' ability to accurately capture these energy variations, a comparison could be made.
4. Correlation: The solvers were assessed by comparing their trajectories with a finely estimated solution. Specifically, the angle between the trajectories generated by the solvers and the quasi-true solution was examined.

By employing these four distinct evaluation methodologies, an analysis of the solvers was conducted, aiding in the selection of the most suitable numerical solver for the subsequent stages of the project.

### 5.2.1 Deviation from fixed points

With  $\mu \in (1, \frac{\theta(\theta+\beta+3)}{\theta-\beta-1})$  the Lorenz system has three fixed points [11]. Meaning that a real solution to the system using any of these points as initial point will stay there as  $t \rightarrow \infty$ . The fixed points for a given value of  $\mu$  are,

$$\begin{aligned} & (0, 0, 0), \\ & (\sqrt{\beta(\mu-1)}, \sqrt{\beta(\mu-1)}, \mu-1), \\ & (-\sqrt{\beta(\mu-1)}, -\sqrt{\beta(\mu-1)}, \mu-1). \end{aligned}$$

To examine how well the numerical solvers can replicate this behaviour we can analyze the numerical approximations of trajectories starting in the fixpoints. To get a good overview we will analyze the results produced by **Algorithm 1** presented below.

---

**Algorithm 1:** Fixpoint stability

---

```
/* Choose  $\beta$ ,  $\theta$ ,  $T$  and  $\Delta t$  */  
1 Create a set  $I$  of different values  $i \in (1, \frac{\theta(\theta+\beta+3)}{\theta-\beta-1})$   
2 for each solver  $s$  do  
3   for each  $i \in I$  do  
4     Set  $\mu = i$   
5     Compute the fixpoints using the values of  $\mu, \beta$  and  $\theta$   
6     for each fixpoint do  
7       Calculate the numerical solution using the solver,  $T, \Delta t$  and the  
     fixpoint as initial condition  
8       error  $\leftarrow$  Calculate the largest distance away from the fixpoint the  
     solution is  
9     Sum all error values  
10 return the sum of all error values for each solver
```

---

### 5.2.2 Convergence for global stability

With  $\mu < 1$  the Lorenz system has a globally stable origin, meaning all solutions to the system will converge towards the origin [1, 11]. We can examine how well a numerical solver can replicate this behaviour by estimating what percentage of numerical trajectories  $\tilde{u}$  starting at a distance  $r$  away from the origin converges towards it. The comparison of the solvers will be done by analyzing the results of **Algorithm 2** below. *global stability ratio*.

---

**Algorithm 2:** Global stability

---

```
/* Choose  $T$  and  $\Delta t$  */  
1 Create a set of points  $V$ , all at a distance  $r$  away from the origin, to use as initial  
  conditions  
2 for each solver do  
3   for each point  $v \in V$  do  
4     Compute the numerical solutions using the solver,  $\Delta t, T$  and  $v$  as initial  
     condition  
5     Determine whether the solutions is closer to the origin than its initial  
     condition.  
6     p  $\leftarrow$  Calculate the percentage of solutions which didn't get closer to the  
     origin.  
7 return the percentages p for each solver
```

---

### 5.2.3 Energy function analysis

We defined an energy function as

$$E(t) = \|\vec{u}(t)\|^2.$$

The behavior of the Lorenz system was examined using this energy function. Three different sets of parameters were used. One set of parameters where the origin was globally stable, one set where the strange attractor did not exist and one where we had a strange attractor. Several initial conditions were chosen close enough to the origin, fixed points or strange attractor for each set of parameters respectively. The energy of the trajectories was then averaged so that one could observe the general trend in energy. The energy average over time was plotted for the different numerical solvers.

### 5.2.4 Correlation

Preferably we would like to be able to compute how “close” the numerical approximations are to the real solutions in the chaotic Lorenz system. This cannot be done however as the non-stationary chaotic solutions cannot be found analytically [4, 5]. Instead an estimation has to be made using a *quasi-true* numerical solution. This solution is one produced by a chosen solver with a relatively small timestep. The measurement of “closeness” used is the *correlation*. Given two trajectories  $\vec{u}(t)$  and  $\vec{y}(t)$  we define the correlation  $C(t)$  as

$$C(t) = \frac{\langle \vec{u}(t), \vec{y}(t) \rangle}{\|\vec{u}(t)\| \|\vec{y}(t)\|}.$$

This measurement tells us, with some limitations, how similar two trajectories are to each other. In  $\mathbb{R}^3$  it represents the *cosine* of the angle between the trajectories at a given time  $t$ . The correlation gives us insight into the chaotic divergence of trajectories by allowing us to observe when two trajectories start diverging from each other and how quickly they do so.

To understand the different solvers’ ability to stay close to a real solution we compute the correlation between their solutions and the quasi-true numerical solutions. To ensure a comprehensive evaluation we do this for several initial conditions and timestep sizes as outlined in **Algorithm 3** below.

---

**Algorithm 3:** Calculating the correlation

---

```
/* Choose endtime  $T$  and a set of points  $P$  */  
1 Create quasittrue numerical solutions using each point in  $P$  as initial point,  $T$  as  
endtime and the solver and timestep which has been chosen to represent a  
quasittrue solution  
2 for each solver do  
3   for each  $\Delta t$  do  
4     Create numerical solutions using each point in  $P$  as initial point,  $T$  as  
     endtime, the solver s and timestep  $\Delta t$   
5     for each  $p \in P$  do  
6        $C \leftarrow$  compute the correlation between a numerical solution and the  
       quasi-true solution for a given initial condition  $p$  for some chosen  $t$ 's.  
7      $C_{avg} \leftarrow$  compute the arithmetic mean of the correlation vectors  $C$  at each  
      $t$ .  
8 return the  $C_{avg}$  vector for each solver and  $\Delta t$ 
```

---

### 5.3 Time dependent $\mu$

To test the stability of the strange attractor we consider the parameter  $\mu$  as being time dependent. Letting  $\mu = \mu(t)$  be some differentiable function with bounded amplitudes we let

$$\mu(t) = \mu_0 + \mu_1 \sin \omega t$$

Where  $\mu_0, \mu_1, \omega \in \mathbb{R}$ . The parameters  $\mu_0, \mu_1$  and  $\omega$  will be varied to find new manifolds the system can live on. The trajectories are plotted for visualization.

### 5.4 Perturbations and stability of manifolds

To assess the stability of the obtained manifolds when allowing  $\mu$  to vary with time ( $\mu = \mu(t)$ ), we conduct a correlation measurement. This involves applying different amplitudes of perturbation to  $\mu$ . The perturbation of  $\mu$  is described as follows:

$$\mu(t) = \mu_0 + \mu_1 \sin \omega t + \varepsilon \cdot \mu'(t)$$

Where  $\mu'(t)$  is some continuously differentiable function. We have previously observed that  $\mu(t)$  in the form of  $\mu(t) = \mu_0 + \mu_1 \sin(\omega t)$  yields an intriguing collection of manifolds. Now, we aim to test the effects of perturbing functions  $\mu'(t)$ . One that is increasing and one

that is bounded. A correlation measurement will be performed for the bounded perturbing function.

## 6 Results

First, we present the result pertaining to the numerical solvers, then, we present the discovered manifolds and their stability.

### 6.1 Parameter selection

Unless otherwise specified, the default selection for the parameters  $\theta$  and  $\beta$  will be  $\theta = 10$  and  $\beta = 8/3$ . These specific values were chosen due to their historical significance, as they were the parameters employed by Lorenz in 1963. Additionally, this parameter choice has remained widely adopted in subsequent studies, establishing it as a commonly used set of parameters.

#### 6.1.1 Energy

For the global stability case  $\mu = 1/2$ , a starting radius for the initial conditions of  $r = 100$  was chosen. For the strange attractor case  $\mu = 28$  and the radius from the origin was again  $r = 100$ . For the fixed point case  $\mu = 23.5$  and a staring radius from the fixed point was chosen to be  $r = 1$ . For all of these different cases an endtime of  $T = 50$  and a timestep of  $\Delta t = 10^{-3}$  was used.

#### 6.1.2 Correlation

To use the algorithm described in 5.2.4 to calculate correlation we want to define a set of initial conditions. The set we use is a 3D grid  $P$  defined as

$$P = \{(x, y, z) : x \in X, y \in Y, z \in Z\}, \quad (2)$$

$$X = \{x \mid x_{i+1} = x_i + \Delta x, i = 0, 1, \dots N_x\},$$

$$Y = \{y \mid y_{j+1} = y_j + \Delta y, j = 0, 1, \dots N_y\},$$

$$Z = \{z \mid z_{k+1} = z_k + \Delta z, k = 0, 1, \dots N_z\}.$$

We set  $x_0 = y_0 = -50, z_0 = -30, \Delta x = \Delta y = \Delta z = 10$  and  $N_x = N_y = N_z = 11$ . These values are chosen since our analysis will be related to trajectories near the attractor of the Lorenz system. Using these values the chosen set  $P$  creates a 3D grid which contains the attractor. To be able to use the algorithm we also want to choose how we calculate the

quasi-true solutions. We chose to do it using the solver RadauIIA5 with a timestep of  $\Delta t = 10^{-5}$ .

## 6.2 Comparison Numerical Solvers

### 6.2.1 Global stability

To ensure the origin is globally stable, we choose  $\mu = 1/2$ . The examined distances  $r$  to the origin were  $r = 10^i$  where  $i = 2, 3, \dots, 8$ . Time step size  $\Delta t = 0.001$ . The values in the plot are the percentage of trajectories that converged to the origin.

Table 6.1: The *global stability ratio* for different  $r$ -values and the different solvers. Using  $\Delta t = 0.001$

<b>r</b>	EF	RK4	MsDTM	Ro5	Ra5
$10^2$	1.0	1.0	1.0	1.0	1.0
$10^3$	0.015	1.0	1.0	1.0	1.0
$10^4$	0.0	0.26	0.19	1.0	1.0
$10^5$	0.0	0.02	0.01	0.995	1.0
$10^6$	0.0	0.0	0.0	1.0	0.94
$10^7$	0.0	0.0	0.0	1.0	0.965
$10^8$	0.0	0.0	0.0	1.0	0.995

### 6.2.2 Fixpoint stability

The maximum deviation, rounded to  $10^{-16}$ , from the fixed points was calculated using end time  $T = 50$  and varying  $\mu$ . It was observed that all solvers remained at the fixed point when the initial condition was set to the same value as the fixed point.

### 6.2.3 Energy

#### Energy of globally stable system

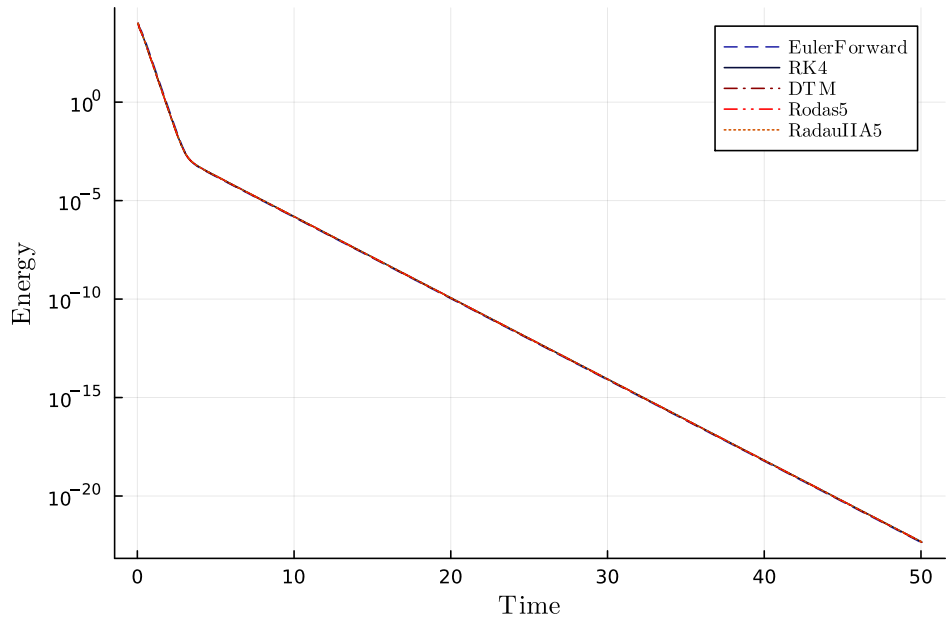


Figure 6.1: Plot of the value of the energy function, defined in section 5.2.3, over time. The parameter values are selected so that the origin is globally stable.

### Energy of chaotic system

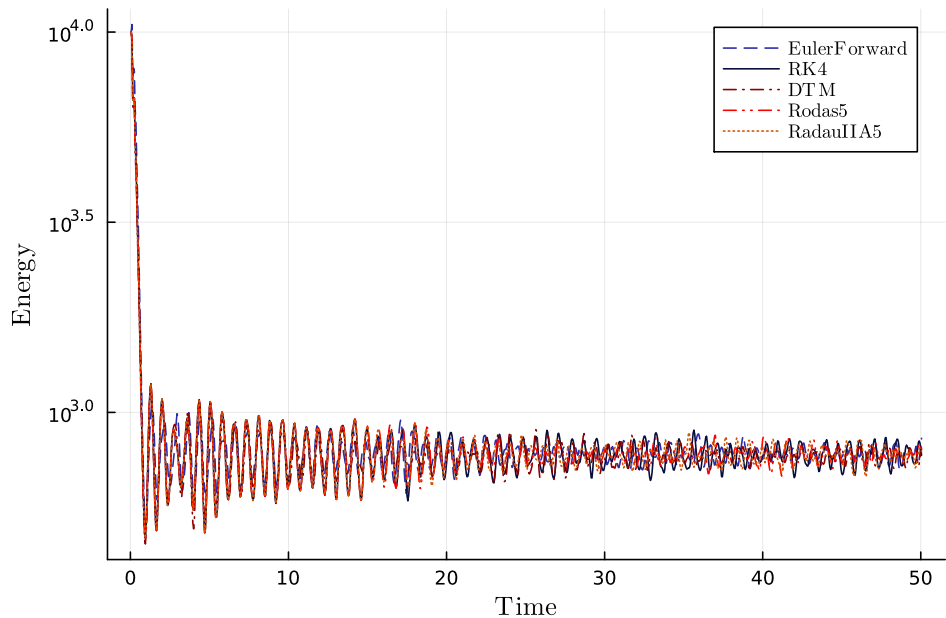


Figure 6.2: Plot of the value of the energy function, defined in section 5.2.3, over time. The parameter values were selected such that the system is chaotic.

## Energy of fixed points

The energy for every solver oscillated rapidly when near the fixpoints, as seen in fig. .2 in the appendix, resulting in a graph which is hard to analyze. Therefore we chose to visualize this result a bit differently.

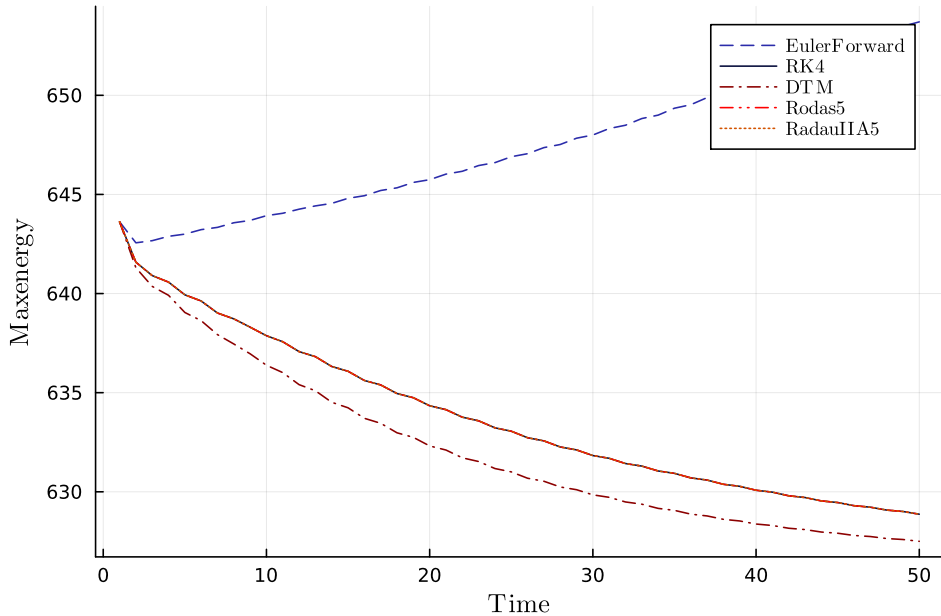


Figure 6.3: Plot of the maximum value of the energy function, defined in section 5.2.3 for each timeintervall of size 1. Initial condition close to a fixpoint of the system.

### 6.2.4 Correlation

These plots were obtained from the correlation scheme.

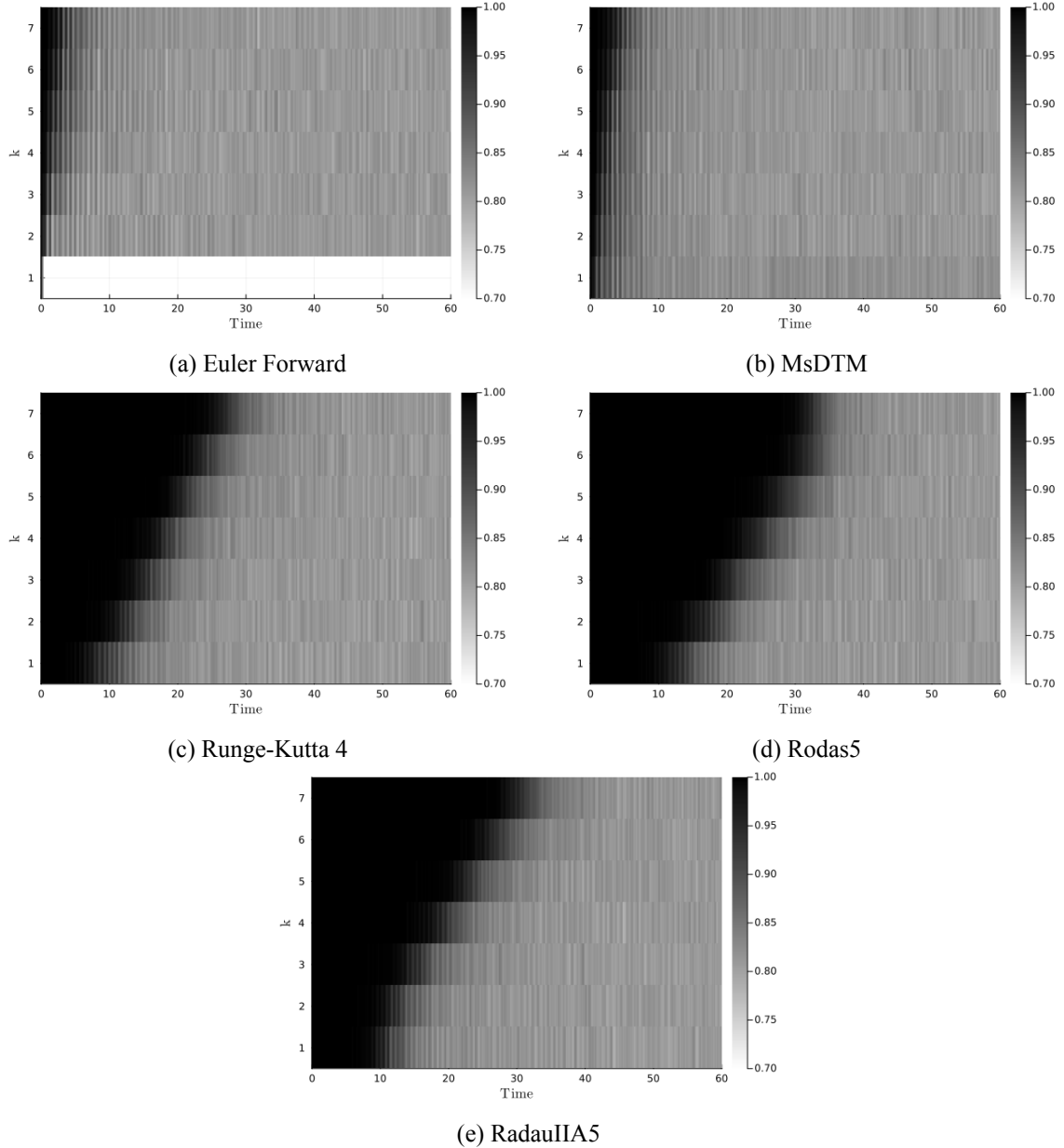


Figure 6.4: The average correlation between the different numerical methods and non-adaptive RadauIIA5 with its step-size  $\Delta t = 10^{-5}$  for different  $k$  values as described in the parameter selection section.

### 6.3 Finding manifolds and perturbing them

Under the parameter function  $\mu(t) = \mu_0 + \mu_1 \sin \omega t$ , several types of manifolds were discovered. Among them, two were observed to be closed, while the remaining two were open. For all manifolds  $\mu_0 = 19$  and  $\mu_1 = 5$ . The frequencies  $\omega$  varied however.  $\omega = 2\pi, 1, 0.001, 50$  exhibited interesting manifolds. When adding an increasing function  $\mu'(t) = 10^{0.02t}$  all manifolds lost their shape but in various different ways.

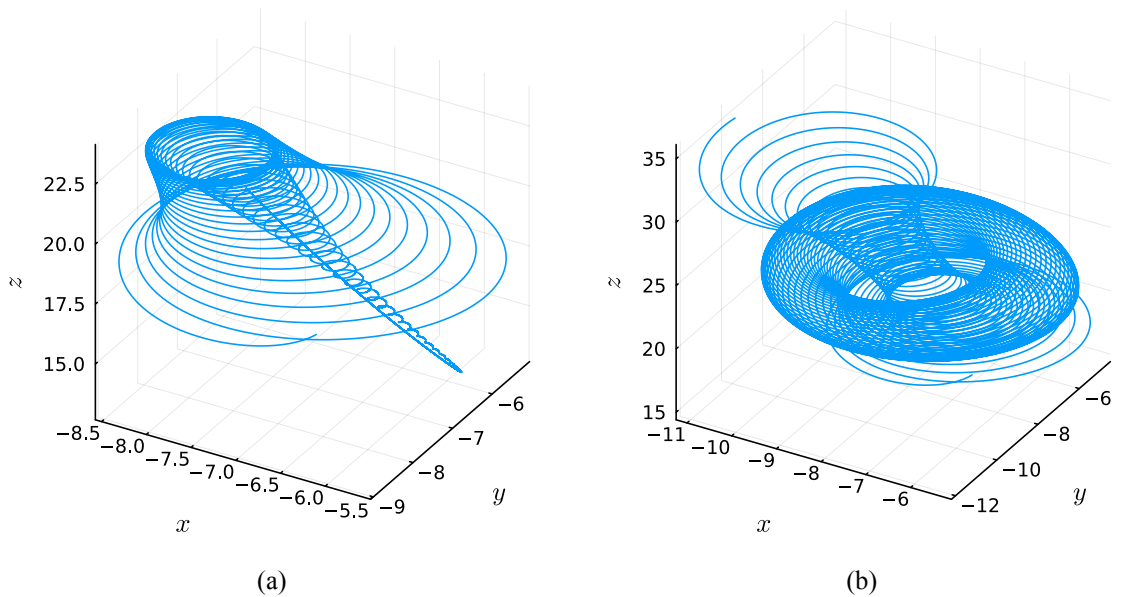


Figure 6.5: In fig. 6.5a  $\mu(t) = 19 + 5 \sin 0.01t$  and the trajectory resembles a volcano. Over time the trajectory converges to the fixed point. Initial condition  $\vec{u}(0) = (-7, -7, 15)$ . This manifold was only found for certain initial conditions. In fig. 6.5b the “Volcano” demonstrates a doughnut-shaped behavior with an increasing parameter value of  $\mu = 19 + 5 \sin(0.01t) + 10^{0.02t}$ . As time progresses the trajectory finds the strange attractor. The initial condition remains  $\vec{u}(0) = (-7, -7, 15)$ .

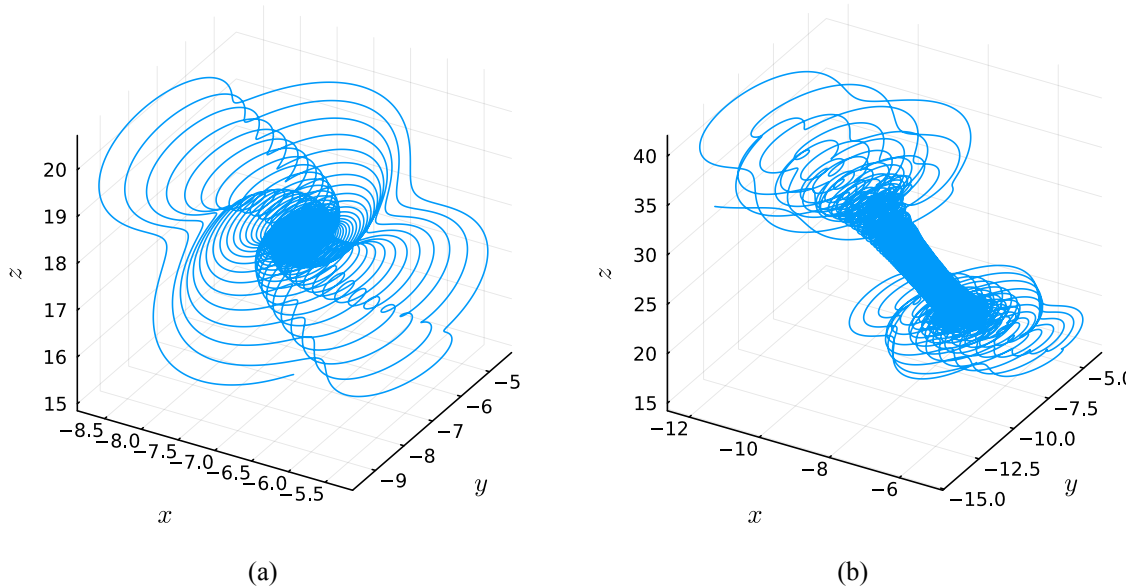


Figure 6.6: A wrinkled napkin-like shape emerges when  $\mu(t) = 19 + 5 \sin 50t$ . As time progresses, the trajectory gradually converges towards a fixed point. The napkin behavior was observed for a range of higher frequencies. In fig. 6.6b the “wrinkled napkin” shoots off,  $\mu(t) = 19 + 5 \sin 50t + 10^{0.02t}$ . As  $t \rightarrow \infty$  it finds the strange attractor.

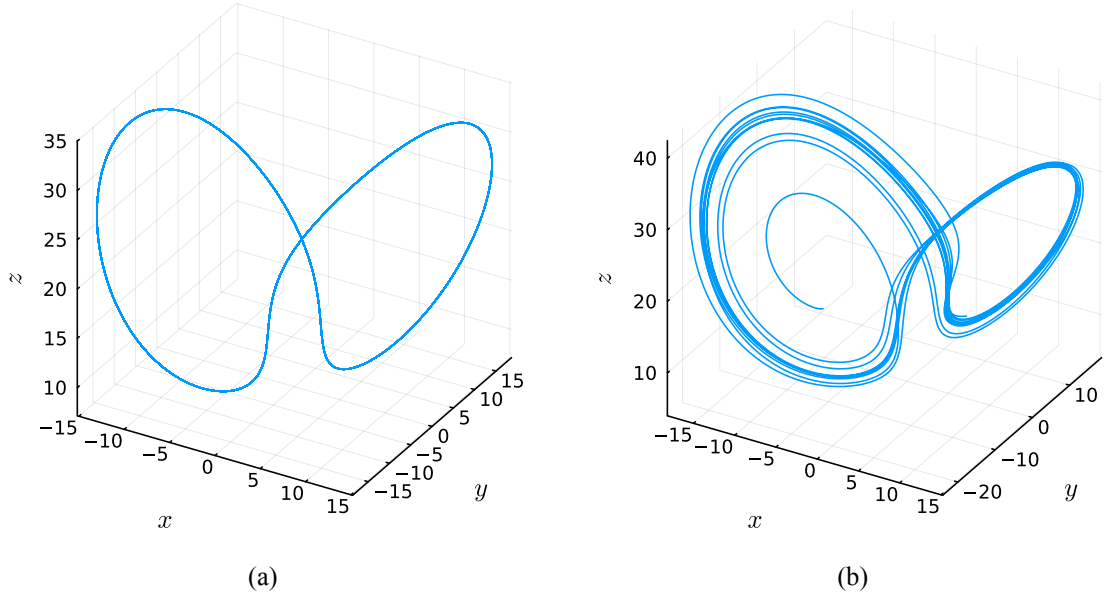


Figure 6.7: In fig. 6.7a, the function for  $\mu(t)$  is given as  $\mu(t) = 19 + 5 \sin(2\pi t)$ . The trajectory resembles the shape of an eight lying down. In fig. 6.7b, the shape of the eight, is perturbed by the addition of another term to  $\mu(t)$ . The equation for  $\mu(t)$  in this case becomes  $\mu(t) = 19 + 5 \sin(2\pi t) + 10^{0.02t}$ .

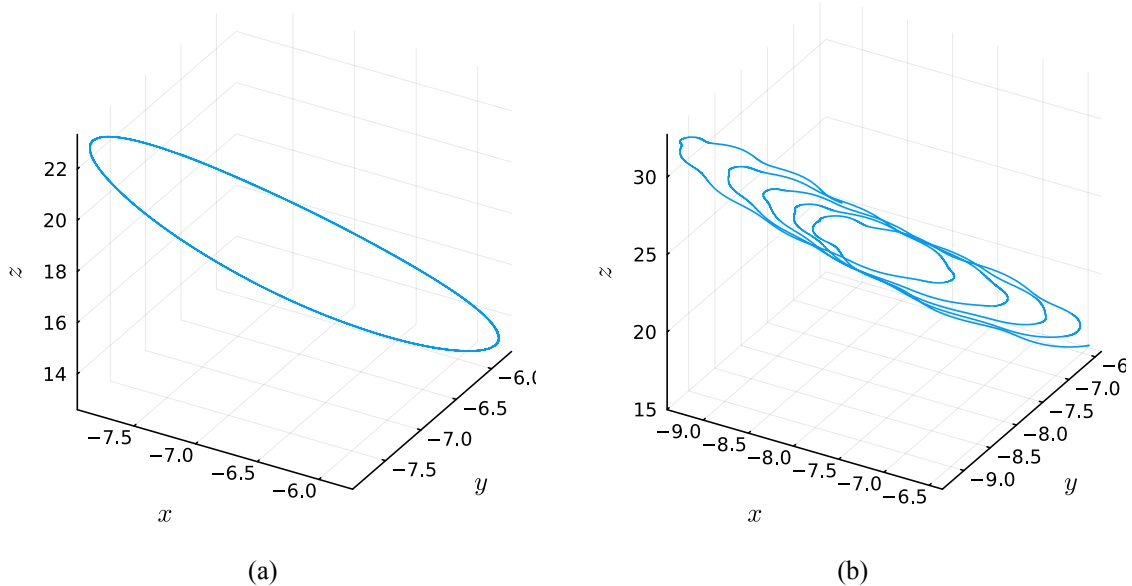


Figure 6.8: In fig. 6.8a, we can observe the trajectory exhibiting an elliptical shape when  $\mu(t) = 19 + 5 \sin t$ . Initial condition  $\vec{u}(0) = (3.98538, 6.0273, 7.95332)$ . In fig. 6.8b, we witness the perturbation effect on the “ellipse”, caused by the additional term  $\mu(t) = 19 + 5 \sin t + 10^{0.02t}$ .

## 6.4 Sensitivity analysis of manifolds

The “eight” shape was chosen for a stability analysis. A bounded function  $\mu'(t) = \sin^2 t$  was chosen to test stability. For the bounded function amplitudes,  $\varepsilon$ , were 1, 1.5, 2, 2.5 and 3.

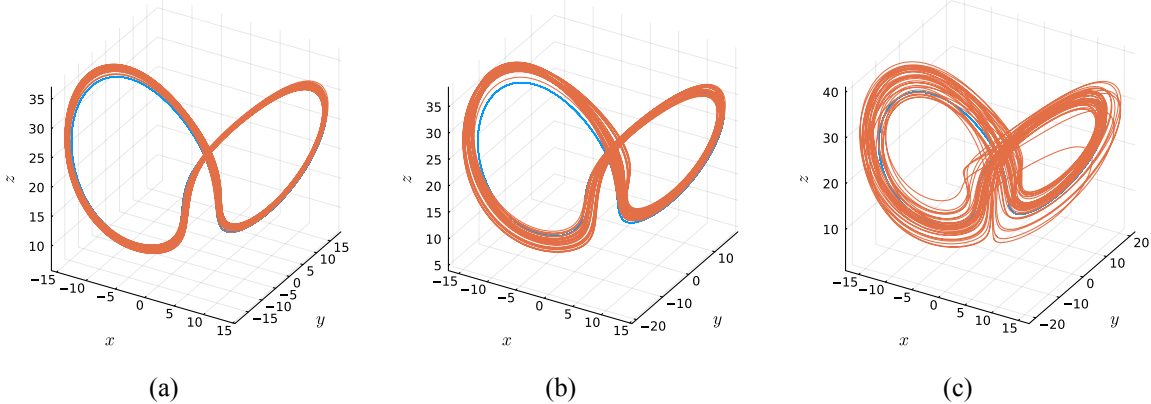


Figure 6.9: The blue trajectory in each subplot is the “eight” manifold given by  $\mu(t) = 19 + 5 \sin 2\pi t$ . In fig. 6.9a the orange trajectory has  $\mu(t) = 19 + 5 \sin 2\pi t + \sin^2 t$ . In fig. 6.9b and fig. 6.9c  $\mu(t) = 19 + 5 \sin 2\pi t + 2 \sin^2 t$  and  $\mu(t) = 19 + 5 \sin 2\pi t + 3 \sin^2 t$  respectively.

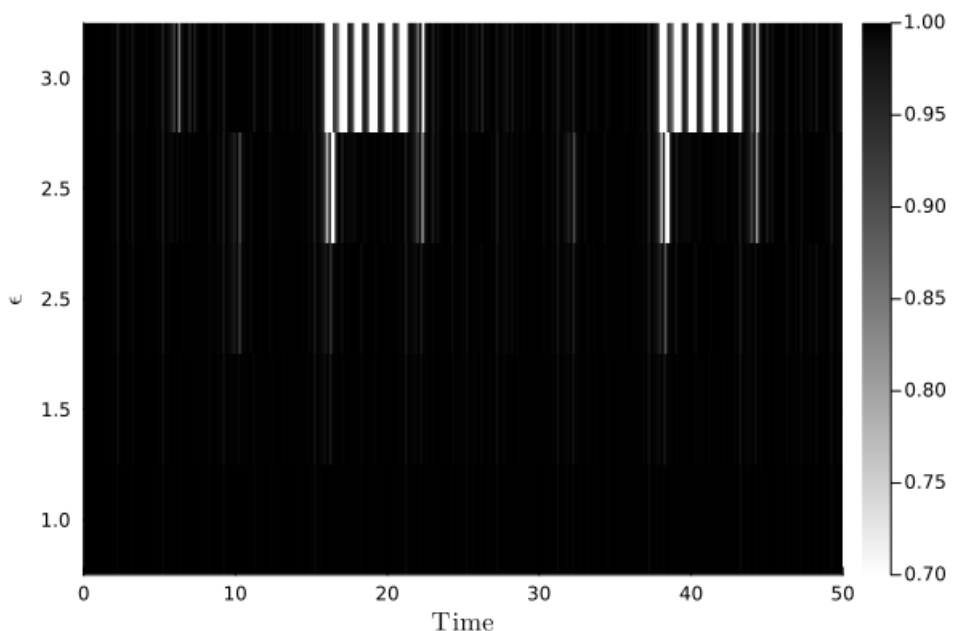


Figure 6.10: The plot displays the correlation between a perturbed and unperturbed version of the “eight” shape,  $\mu(t) = 19 + 5 \sin 2\pi t$ . The perturbation is caused by the function  $\mu'(t) = \sin^2 t$ . The range of  $\varepsilon$  values spans from 1 to 3. Regardless of the specific  $\varepsilon$  value, the minimum bound for  $\mu$  remains at 14, indicating that the system is consistently in a chaotic state. However, as  $\varepsilon$  increases to 3, a deterioration in correlation becomes evident. At this level, the upper bound of  $\mu(t)$  reaches 27.

## 7 Discussion

### 7.1 Comparison Numerical Solvers

#### 7.1.1 Global stability

Among the numerical methods tested, Euler Forward, Runge-Kutta 4, and MsDTM exhibited notably inferior performance compared to Rodas5 and RadauIIA5. The poor performance of the Euler Forward method can be attributed the large second-order derivative of the Lorenz system far from the origin, resulting in significant local truncation errors. Runge-Kutta 4 and MsDTM, being higher-order methods, demonstrated improved performance over Euler Forward. However, for distances from the origin larger than  $10^3$ , their reliability diminished. In contrast, RadauIIA5 and Rodas5 consistently performed well even for larger time steps. Their superior performance can be attributed to their A-stability and higher order compared to the other methods tested. Although RadauIIA5 and Rodas5 outperformed the rest in this particular test, it is worth noting that most of the trajectories in this research project are not expected to deviate significantly from the origin. Therefore, the convergence of Runge-Kutta 4 and MsDTM should suffice for our purposes.

#### 7.1.2 Energy

##### Energy of globally stable system

According to theory, when  $\mu$  is set to a value less than 1, trajectories originating from any initial condition should converge towards the origin. As we employed the squared distance to the origin as our energy measure, we expected it to approach zero. In line with our expectations, the energy values did approach zero for the various solvers when a relatively small time step of  $\Delta t = 0.001$  and a radius of  $r = 250$  were used. Notably, when examining the energies, it appeared that all solvers demonstrated exponential convergence towards machine precision zero.

##### Energy of fixed points

Except for the Euler Forward solver, all the solvers exhibit a similar pattern of convergence towards the fixed point. As seen in section 6.2.3 and fig. .1, these solvers demonstrate oscillations with diminishing amplitude centered around a specific energy value. In

contrast, the Euler Forward solver does not converge; rather, it appears to diverge from the energy value associated with the fixed point. This behavior can likely be attributed to the Euler Forward method being a first-order method.

### Energy of chaotic system

As observed in section 6.2.3, all the solvers demonstrate rapid convergence towards an energy value below  $10^3$  to subsequently oscillate around it. When a trajectory becomes trapped in the strange attractor, it remains confined within a bounded region while continuously in motion. Consequently, the energy of such a trajectory tends to fluctuate around a specific value. Considering that all solvers exhibit this characteristic behavior, it is highly probable that they have converged towards the strange attractor.

#### 7.1.3 Fixpoint stability

None of the solvers produced any significant deviation. In this test no significant difference between the solvers was found.

#### 7.1.4 Correlation

Upon examining the correlation plots in section 6.2.4 with the black-colored regions indicating the correlation time, it is evident that Rodas5, RadauIIA5, and Runge-Kutta 4 exhibit the longest periods of correlation with the quasi-true solution. In contrast, the other two solvers demonstrate comparatively poorer performance in terms of correlation.

All solvers achieve longer correlation times as the time steps decrease, with the exception of Rodas5 at the smallest time step as seen in fig. 6.4d. Surprisingly, for this particular time step, no improvement in correlation is observed compared to the previous step. Furthermore, even with an even finer time step of  $2 \cdot 10^{-5}$ , the correlation time does not appear to improve as can be seen in fig. .2 in the appendix. This suggests the existence of a limit on how long a solver can maintain correlation with the quasi-true solution.

We propose two possible explanations for this phenomenon. The first explanation is that we may have reached the limitations of the quasi-true solution itself. Since the quasi-true solution is also a numerical estimation, its accuracy diminishes over time. Once the fine solution starts diverging from the true solution, assuming correlation with another numerical solver would no longer be valid. The second explanation we propose involves

the error in the Rodas5 trajectory being errors arising from computer precision. In addition to the errors introduced by the numerical scheme, there is a rounding error associated with each step of the algorithm due to accuracy of the use of double precision memory. In our calculations, the rounding error is approximately on the order of  $10^{-16}$ . This rounding error accumulates at each time step, meaning that regardless of how small the error caused by the scheme itself is, there is a nonzero lower limit to the overall error of the numerical solution. Consequently, there may come a point in time where, for all methods, the accumulated rounding errors cause the trajectory to consistently diverge from the true solution. While the errors of the numerical methods should dominate for larger time steps, for smaller time steps, the increased number of total steps amplifies the significance of rounding errors [5].

Furthermore, in addition to considering correlation, the computational time required by each method should also be taken into account. Although not precisely quantified, Rodas5 and RadauIIA5 require significantly more time to generate numerical solutions compared to the other methods. Given that Runge-Kutta 4 performs well across all tests, it is chosen as the preferred method for subsequent analyses in this thesis.

## 7.2 Finding manifolds and perturbing them

Four distinct manifolds were found showing that the parameter  $\mu$  can be used to control the system. When an increasing function  $\mu'(t) = 10^{0.02t}$  was added, the manifolds lost their original shape. The specific manner in which this transformation occurred varied, making the study of their trajectory towards losing the manifold shape particularly intriguing.

## 7.3 Sensitivity analysis of manifolds

When considering the “eight” shape with  $\mu(t) = 19 + 5 \sin(2\pi t)$ , there exists a set of functions  $\mu(t) = 19 + 5 \sin(2\pi t) + \varepsilon \cdot \mu'(t)$  that still preserve a similar manifold structure. However, one could argue that the “eight” shape already bears resemblance to the strange attractor, and if the system were to converge to the strange attractor at higher  $\mu(t)$  values, the correlation would remain strong. Notably, when  $\varepsilon = 3$ , the resulting plotted shape more closely resembles the strange attractor than the original “eight” shape.

## 8 Future Work

For future research, it would be worthwhile to explore a problem formulated in the following manner. Consider a differential equation with an infinite-dimensional parameter  $\phi := \phi(s) \in \mathcal{X}$ :

$$\begin{cases} \frac{d\vec{u}}{dt} = f(\vec{u}, \phi(s)), \\ \vec{u}(0) = \vec{u}_0. \end{cases}$$

Suppose our objective is to minimize a cost functional defined as

$$\mathcal{J}(\phi(s)) = \lim_{t \rightarrow \infty} \frac{1}{T} \int_0^T \mathcal{J}(\vec{u}(t), \phi(s)) dt,$$

where we are interested in finding solutions that lie on a specific manifold. To enforce constrained optimization, we can utilize techniques based on adjoint-calculus. In this case, we consider the problem:

$$\min_{\phi \in \mathcal{X}} \mathcal{J}(\phi)$$

subject to  $C(\vec{u}(\phi), \phi) = 0$ , where the constraint is defined by a manifold  $\mathcal{M} := \{\phi \in \mathcal{X} : C(x(\phi), \phi) = 0\}$ .

Traditional optimization methods often struggle to handle the chaotic divergence of trajectories, rendering standard gradient descent unsuitable. This is where the Shadowing Lemma and the LLS (Local Linearization and Subspace) method come into play. By employing these techniques, we can overcome these challenges and make progress in solving the problem effectively. [5]

It is further interesting to continue exploring other manifolds and their respective stability.

## References

- [1] Cantisán, Julia, Seoane, Jesús, and Sanjuán, Miguel. “Transient dynamics of the Lorenz system with a parameter drift”. In: *International Journal of Bifurcation and Chaos* (Sept. 2020). DOI: <https://www.researchgate.net/publication/344360925>.
- [2] Ernst Hairer, Gerhard Wanner. *Solving Ordinary Differential Equations II*. eng. Second edition. Springer Berlin, Heidelberg, 1996. ISBN: 978-3-642-05221-7.
- [3] Gad, Emad et al. “A-Stable and L-Stable High-Order Integration Methods for Solving Stiff Differential Equations”. In: *IEEE Transactions on Computer-Aided Design of Integrated Circuits and Systems* 28.9 (2009), pp. 1359–1372. DOI: 10.1109/TCAD.2009.2024712.
- [4] Lorenz, Edward N. “Deterministic Nonperiodic Flow”. In: *Journal of Atmospheric Sciences* 20.2 (1963), pp. 130–141. DOI: 10.1175/1520-0469(1963)020<0130:DNF>2.0.CO;2. URL: [https://journals.ametsoc.org/view/journals/atsc/20/2/1520-0469\\_1963\\_020\\_0130\\_dnf\\_2\\_0\\_co\\_2.xml](https://journals.ametsoc.org/view/journals/atsc/20/2/1520-0469_1963_020_0130_dnf_2_0_co_2.xml).
- [5] Matharu, Pritpal. personal communication. May 5, 2023.
- [6] Munganga, Justin et al. “Introduction of the differential transform method to solve differential equations at undergraduate level”. In: *International Journal of Mathematical Education in Science and Technology* 45 (Dec. 2014). DOI: 10.1080/0020739X.2013.877609.
- [7] Pilugin, Sergei Ju. *Shadowing in dynamical systems*. New York: Springer, 1999. ISBN: 3-540-66299-5.
- [8] Sauer, Tim. *Numerical analysis*. eng. Third edition. Pearson, 2018. ISBN: 9780134696454.
- [9] Simmons, George F. *Differential equations with applications and historical notes*. Third Edition. Chapman amp; Hall/CRC, 2016.
- [10] Spoto, Federica and Milani, Andrea. “Shadowing Lemma and chaotic orbit determination”. In: *Celestial Mechanics and Dynamical Astronomy* 124.3 (Dec. 2015), pp. 295–309. DOI: 10.1007/s10569-015-9667-7. URL: <https://doi.org/10.1007%2Fs10569-015-9667-7>.

- [11] Strogatz, Steven H. (Steven Henry). *Nonlinear Dynamics and Chaos : With Applications to Physics, Biology, Chemistry, and Engineering*. eng. Second edition. Studies in nonlinearity. Boca Raton, FL: CRC Press, 2018. ISBN: 0-429-68015-5.

## **Appendices**

## Correlation of finer solution

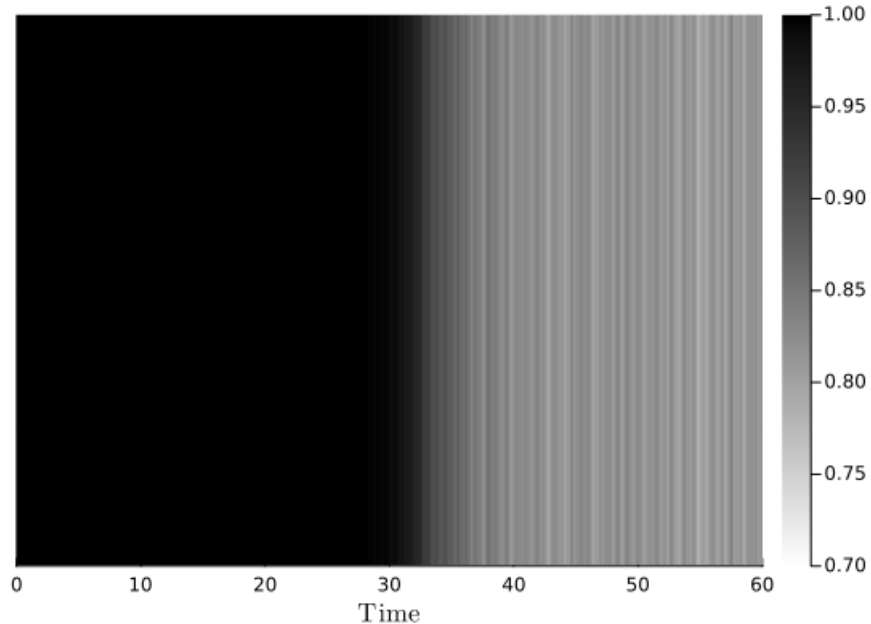


Figure .1: Correlation using Rodas5 with a timestep corresponding to k=8

## Energy plot of fixpoint

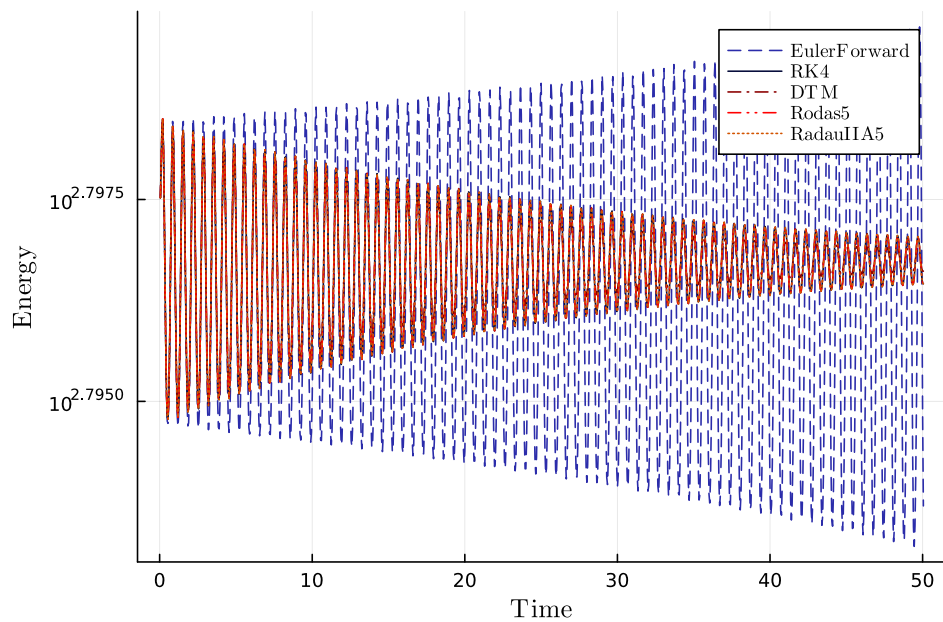


Figure .2: Caption

## Stabilities

To measure if a numerical solver is stable one studies the equation [3]:

$$\frac{dx}{dt} = \lambda x(t)$$

Where  $\lambda \in \mathbb{C}^- = \{\lambda \in \mathbb{C} | \Re(\lambda) < 0\}$ . The solution to this system is  $x = e^{\lambda t}$  and  $x \rightarrow 0$  as  $t \rightarrow \infty$ . A numerical solver is A-stable if  $|x_i| < |x_j|$  for each  $i > j$  where  $x_i$  is the numerical solution at  $t = t_i$ . The solution is L-stable if  $\lambda \in \mathbb{C}^- \cup \infty$ . A Runge-Kutta method is B-stable if

$$\langle f(u) - f(\hat{u}), u - \hat{u} \rangle \leq 0 \implies \|u_1 - \hat{u}_1\| \leq \|u_0 - \hat{u}_0\|$$

Where  $u_1$  and  $\hat{u}_1$  are the numerical approximations of the Runge-Kutta method after one iteration with initial condition  $u_0$  and  $\hat{u}_0$  and  $\frac{du}{dt} = f(u)$  [2].